Hydrogen Selective SiCH Inorganic–Organic Hybrid/γ-Al2O3 Composite Membranes

Miwako Kubo, Ryota Mano, Misako Kojima, Kenichi Naniwa, Yusuke Daiko, Sawao Honda, Emanuel Ionescu, Samuel Bernard, Ralf Riedel, Yuji Iwamoto

membranes

MDPI

Article

Hydrogen Selective SiCH Inorganic–Organic Hybrid/γ-Al_2O_3 Composite Membranes

Miwako Kubo [1], Ryota Mano [1], Misako Kojima [1], Kenichi Naniwa [1], Yusuke Daiko [1], Sawao Honda [1], Emanuel Inonescu [2], Samuel Bernard [3], Ralf Riedel [2] and Yuji Iwamoto [1,*]

1 Department of Life Science and Applied Chemistry, Graduate School of Engineering, Nagoya Institute of Technology, Gokiso-cho, Showa-ku, Nagoya 466-8555, Japan; m.kubo.579@stn.nitech.ac.jp (M.K.); mlikeplaypianor@i.softbank.jp (R.M.); m.kojima.811@stn.nitech.ac.jp (M.K.); k.naniwa.270@stn.nitech.ac.jp (K.N.); daiko.yusuke@nitech.ac.jp (Y.D.); honda@nitech.ac.jp (S.H.)
2 Institut für Materialwissenschaft, Technische Universität Darmstadt, Otto-Berndt-Str. 3, 64287 Darmstadt, Germany; ionescu@materials.tu-darmstadt.de (E.I.); ralf.riedel@tu-darmstadt.de (R.R.)
3 CNRS, IRCER, UMR 7315, University of Limoges, F-87000 Limoges, France; samuel.bernard@unilim.fr
* Correspondence: iwamoto.yuji@nitech.ac.jp; Tel.: +81-52-735-5276

Received: 28 August 2020; Accepted: 24 September 2020; Published: 25 September 2020

Abstract: Solar hydrogen production via the photoelectrochemical water-splitting reaction is attractive as one of the environmental-friendly approaches for producing H_2. Since the reaction simultaneously generates H_2 and O_2, this method requires immediate H_2 recovery from the syngas including O_2 under high-humidity conditions around 50 °C. In this study, a supported mesoporous γ-Al_2O_3 membrane was modified with allyl-hydrido-polycarbosilane as a preceramic polymer and subsequently heat-treated in Ar to deliver a ternary SiCH organic–inorganic hybrid/γ-Al_2O_3 composite membrane. Relations between the polymer/hybrid conversion temperature, hydrophobicity, and H_2 affinity of the polymer-derived SiCH hybrids were studied to functionalize the composite membranes as H_2-selective under saturated water vapor partial pressure at 50 °C. As a result, the composite membranes synthesized at temperatures as low as 300–500 °C showed a H_2 permeance of 1.0–4.3 × 10^{-7} mol m^{-2} s^{-1} Pa^{-1} with a H_2/N_2 selectivity of 6.0–11.3 under a mixed H_2-N_2 (2:1) feed gas flow. Further modification by the 120 °C-melt impregnation of low molecular weight polycarbosilane successfully improved the H_2-permselectivity of the 500 °C-synthesized composite membrane by maintaining the H_2 permeance combined with improved H_2/N_2 selectivity as 3.5 × 10^{-7} mol m^{-2} s^{-1} Pa^{-1} with 36. These results revealed a great potential of the polymer-derived SiCH hybrids as novel hydrophobic membranes for purification of solar hydrogen.

Keywords: allyl-hydrido-polycarbosilane (AHPCS); organic–inorganic hybrid; hydrophobicity; membrane; hydrogen separation; hydrogen affinity; polymer-derived ceramics (PDCs)

1. Introduction

Hydrogen (H_2) is an attractive energy carrier because of its high energy yield of 120 J g^{-1}. This value is about 2.8 times higher than hydrocarbon fuels [1]. Moreover, the combustion product is water and thus completely clean in a carbon dioxide (CO_2)-neutral manner.

In addition to the current hydrogen production by the steam reforming of naphtha and methane, hydrogen can be produced using several resources including hydropower, nuclear energy and renewable energy sources like biomass, wind, geothermal and solar. Among them, hydrogen production via photoelectrochemical (PEC) water-splitting has received increased attention as an environmental-friendly and low-cost solar-to-hydrogen pathway because of its potential for high conversion efficiency at low operating temperatures using cost-effective semiconductor-based photoreaction catalysts [2–4].

The solar hydrogen production systems are expected to be used in terms of global-warming prevention and a stable supply of energy. Therefore, in Japan, the research and development of these systems have been promoted by the Ministry of Economy, Trade and Industry (METI). For example, as an ongoing New Energy and Industrial Technology Develop Organization (NEDO) R&D project, the "Artificial Photosynthesis" Project has been conducted by the Japan Technological Research Association of Artificial Photosynthetic Chemical Process (ARPChem) [5,6]. This project is composed of three research teams: the Solar Hydrogen Team for water photo-splitting catalysts, the Hydrogen Separation Team for gas separation membranes and the Synthetic Catalyst Team for CO_2 hydrogenation catalysts. All teams are concentrating in materials research and development. These teams also have their missions for future planning and designing industrial photocatalytic plants, gas separation systems with safety measures against explosion, and catalytic synthesis plants, respectively [5,6].

The PEC reaction simultaneously generates H_2 and oxygen (O_2) by an oxidation–reduction reaction of water under sunlight in the presence of semiconducting catalysts

$$2H_2O \rightarrow 2H_2 + O_2 \quad (1)$$

Since H_2 and O_2 react in a large range of H_2 concentration of 4–95% [7], this hydrogen production system requires an efficient separation technology for purifying H_2 from the syngas containing O_2.

There are several candidate technologies for H_2 purification such as cryogenic distillation, PSA (pressure swing adsorption) and membrane separation. Among them, membrane separation shows some advantages including energy efficiency and simple separation schemes suitable for establish safe operation process for purification of solar H_2.

However, under the given operating conditions [5,6,8], it is difficult to apply conventional H_2-selective membranes, which require higher operation temperatures, approximately above 90, 180 and 350 °C for polymer [9], silica [10–12] and metal membranes [13–15], respectively. There are also technical issues such as water-induced swelling for polymer membranes, lower H_2 permeance for supported liquid membranes [16–18] and gas permeability degradation for intrinsically hydrophilic silica-based membranes [8,19,20].

Recently, increasing attention has been directed to organic–inorganic hybrid materials as promising functional materials in various fields such as optics, electronics and energy. Synergistic properties of hybrid materials can be achieved by harmonizing advantageous properties of an organic component, such as solubility, plasticity and hydrophobicity, with those of an inorganic component such as high strength and thermal and/or chemical stability [21,22]. The polymer-derived ceramics (PDCs) route [23,24] appears to be an efficient approach for the synthesis of novel organic–inorganic hybrids categorized as Class II hybrids according to the classification given by Sanchez [25], where the organic and inorganic components are linked together by strong chemical bonds, by polymerization and thermal or chemical cross-linking of silicon-based polymers. Moreover, this process can provide a means to vary the specific properties of the silicon-based polymers such as solubility and viscosity, which provides the versatility in shaping capabilities including the formation of surface coatings and membranes similar to those successfully achieved with hydrocarbon-based polymers. In the topic of PDCs, polycarbosilanes (PCSs) are well known as precursors for silicon carbide (SiC)-based ceramics [26,27]. Their synthesis by the Kumada rearrangement of polydimethylsilane (PDS) has been reported by Yajima et al. [26]. Since polymer-derived amorphous silicon (oxy)carbide (SiC and SiCO) show excellent thermal and chemical stabilities [28,29], PDS [30], PCSs [31–37] and PCS derivatives such as allyl-hydro-polycarbosilane (AHPCS) [38–42] have been applied as precursors of microporous amorphous SiOC [30–34] and SiC [29,35–42] membranes to investigate their gas permeation properties mainly at high temperatures, $T \geq 200$ °C. PCSs are also appropriate as functional Class II hybrids: The silicon-carbon (Si-C) backbone endows several attractive properties of PCSs such as high flexibility and excellent thermal, chemical and electrical stabilities [43–45]. The hydrocarbon groups attached to the Si-C backbone provide room temperature stability in air and PCSs can be applied as an active binder for the formation of powder compact to fabricate polycrystalline SiC ceramics [46–49]. Moreover, in our

previous study [50], PCSs were found to show an excellent hydrophobic property: gas permeations under highly humid condition at 50 °C of a hydrophilic mesoporous γ-Al_2O_3 membrane were successfully stabilized by modification with SiCH organic–inorganic hybrid via melt impregnation of PCS at 120 °C [50].

In this study, AHPCS was converted to highly cross-linked ternary SiCH organic–inorganic hybrids with enhanced thermal stability and hydrophobicity by heat treatment at temperatures as low as 300–500 °C in argon (Ar). Highly hydrophobic property of the AHPCS-derived SiCH hybrids was characterized by the water vapor adsorption–desorption isotherm measurement at 25 °C. Then, the SiCH organic–inorganic hybrid served to modify a mesoporous γ-Al_2O_3 membrane via dip-coating with AHPCS followed by the heat treatment of the composite at 300–500 °C in Ar.

Single gas permeances of helium (He), hydrogen (H_2) and nitrogen (N_2) under dry condition at 25–80 °C were measured to characterize the intrinsic low-temperature gas permeation properties of the SiCH organic–inorganic hybrid/γ-Al_2O_3 composite membrane. Then, as the primary accelerated degradation test for the suggested solar H_2 purification condition of 10% humidity at 50 °C [5,6], the gas permeance measurements were performed under the saturated water vapor partial pressure at 50 °C. In this measurement, a H_2-N_2 mixed feed gas in the molar ratio 2:1 was used as a simulated syngas produced by the PEC reaction (Equation (1)) in which O_2 (0.346 nm) [51] was replaced by inert N_2 having a similar kinetic diameter (0.364 nm) [51] to avoid explosion accidents. Moreover, for some selected membrane samples and the supported mesoporous γ-Al_2O_3 membrane itself, cyclic gas permeation measurements were continuously performed under water vapor partial pressures ranging from 0 to 1.0 at 50 °C. Effect of the composite membrane synthesis temperature on the hydrophobicity and gas permeation properties under dry and wet conditions were discussed aiming to develop novel hydrophobic membranes for the purification of solar hydrogen at low temperatures around 50 °C.

2. Experimental Procedures

2.1. Preparation of the Supported Mesoporous γ-Al_2O_3 Membrane

Commercially available macroporous α-Al_2O_3 tubular support (6 mm outer diameter, 4 mm inner diameter and 60 mm length, Noritake Co., Ltd., Nagoya, Japan) was used. The α-Al_2O_3 support was composed of a fine outer surface layer (mean pore diameter, d_p = 150 nm) and a core (d_p = 700 nm). Total porosity of the tubular support was 40%. A mesoporous γ-Al_2O_3 membrane was fabricated by dip coating of a boehmite (γ-AlOOH) sol on the α-Al_2O_3 tubular support followed by heat treatment in air at 600 °C for 3 h according to a published procedure [50].

2.2. Modification of a Supported γ-Al_2O_3 Membrane with AHPCS-Derived Organic–Inorganic SiCH Hybrid

Commercially available AHPCS (SMP-10 was provided by Starfire Systems, Inc., Glenville, NY, USA. Anal. Found (wt %): Si, 54.8; C, 35.0; H, 8.3; O, 1.9. FT-IR (ATR/cm^{-1}): ν (C−H) = 3076 (s), 3003 (s), 2958 (s), 2895 (s), 2850 (m), ν(Si−H) = 2123 (vs), δ(allyl) = 1629 (m), δ(CH_2) = 1395 (m), δ(Si-CH_3) = 1251 (s), δ(Si-CH_2-Si) = 1049 (s), δ(Si-H) = 941.1 (s), δ(Si-C) = 854.3 (s), δ(SiCH_3) = 770 (s); ^{1}H NMR (300 MHz, $CDCl_3$, δ/ppm): 0.05 (br, -Si-C**H**$_3$), 0.4 (br, -Si-C**H**$_2$-), 1.56–1.9 (br, -Si-C**H**$_2$-CH=CH_2), 3.4–3.84 (br, -Si**H**$_3$C), 3.8–4.1 (br, -Si**H**$_2$$CH_2$), 4.85–5.05 (br, -Si-$CH_2$-CH=C**H**$_2$), 5.71–5.93 (br, Si-$CH_2$-C**H**=$CH_2$). As a precursor solution for modifying the supported γ-Al_2O_3 membrane, 1 wt % dry xylene (super dehydrated grade, 99.5% purity, Wako Pure Chemical Co., Ltd., Osaka, Japan) solution of as-received AHPCS was prepared under the inert atmosphere of Ar. By following the procedures described in our previous report [50], the AHPCS solution was dip-coated on the supported γ-Al_2O_3 membrane, then dried and heat-treated under flowing Ar at 300, 400 and 500 °C for 1 h at a heating/cooling rate of 100 °C h^{-1} to afford SiCH organic–inorganic hybrid-modified γ-Al_2O_3 membrane placed on the α-Al_2O_3 tubular support (SiCH hybrid/γ-Al_2O_3 composite membrane).

The 500 °C-heat treated membrane was further modified by the melt impregnation of a commercially available PCS at 120 °C under Ar atmosphere (Type L, Nippon Carbon Co., Ltd., Tokyo, Japan) according to the published procedure [50].

2.3. Characterizations

The molecular weight distribution curve of as-received AHPCS was measured at 40 °C by using gel permeation chromatography (GPC, Model ShodexGPC-104 equipped with two tandem columns (Model Shodex LF-404, Showa Denko K.K., Tokyo, Japan) and a refractive index detector (Model Shodex RI-74S, Showa Denko K.K., Tokyo, Japan). The columns were calibrated against polystyrene standards. Tetrahydrofuran (THF, 99.5% purity, Wako Pure Chemical Co., Ltd., Osaka, Japan) was used as the eluent and a flow rate was adjusted to 1.0 mL min^{-1}.

The thermal decomposition and cross-linking behaviors of as-received AHPCS up to 1000 °C was studied by thermogravimetry combined with mass spectrometry (TG-MS) analyses (Model STA7200, Hitachi High Technologies Ltd., Tokyo, Japan/Model JMS-Q1500 GC, JEOL, Tokyo, Japan). The measurements were performed under He atmosphere with a heating rate of 10 °C min^{-1}.

Powder samples of the heat-treated AHPCS were prepared under the same manner for the heat treatment of the supported mesoporous γ-Al_2O_3 membrane after dip-coating of the AHPCS solution.

Fourier transform (FT)-IR spectrum was recorded on the as-received AHPCS and AHPCS-derived powder samples by the potassium bromide (KBr) disk method (Model FT/IR-4200IF, JASCO Corp., Tokyo, Japan). Note that FT-IR spectrum was also recorded on the powder sample of 700 °C-heat treated AHPCS. Raman spectrum was recorded on as-received AHPCS and heat-treated AHPCS (Renishaw, inVia Reflex, New Mills, England).

Hydrophobicity of the heat-treated AHPCS powder samples was characterized by measuring the water vapor adsorption–desorption isotherms at 25 °C (Model BELSORP-aqua 3, MicrotracBEL Corp., Osaka, Japan). The powder samples were pretreated at 120 °C for 6 h under vacuum.

The cross-sectional structure and top surface of the SiCH hybrid/γ-Al_2O_3 composite membrane were observed by a scanning electron microscope (SEM, Model JSM-6360LV, JEOL Ltd., Tokyo, Japan). The distribution of the SiCH hybrid within the composite membrane was examined by the energy dispersive X-ray spectroscopic (EDS) analysis (Model JSM-6010LA mounted on SEM, JEOL Ltd., Tokyo, Japan).

Single gas permeances through the membrane samples under dry conditions were measured for He, H_2 and N_2 by the volumetric method at constant pressure. The setup of the equipment and procedure for the measurements was shown in our previous report [50]. The gas permeances at 25, 50 and 80 °C were measured in the size order of a kinetic diameter for He (0.26 nm), H_2 (0.289 nm) and N_2 (0.364 nm) [51]. The single gas permeance (Q_i) was evaluated by using Equation (2),

$$Q_i = \frac{V}{A(p_H - p_L)} \quad (2)$$

where V (mol s^{-1}) is the permeate molar flow rate, A (m^2) is the membrane area and p_H (Pa) and p_L (Pa) are pressures of the gas feed side and the gas permeate side, respectively. In this study, the ($p_H - p_L$) in Equation (1) was fixed as 100 kPa.

The permselectivity (α) was evaluated by calculating the single gas permeance ratio of two different kinds of gases.

H_2 and N_2 gas permeances under dry and wet condition of the saturated water vapor partial pressure (p/p_0 (H_2O) = 1.0) were measured at 50 °C using a mixed feed gas with a 2:1 molar ratio of H_2 and N_2 as a simulated syngas produced by the PEC reaction. For some selected membranes and the supported mesoporous γ-Al_2O_3 membrane itself, cyclic gas permeation measurements were performed under various p/p_0 (H_2O) ranging from 0 to 1.0 at 50 °C.

The permeate gas composition was analyzed using a gas chromatograph (GC, Model CP-4900 Micro-GC, Varian medical systems Inc., Palo Alto, CA, USA) and Ar sweep gas (50 mL min^{-1}). Each gas

permeance of H_2 and N_2 was calculated using the analyzed composition and the measured mixed gas permeate molar flow rate. The water vapor permeance was evaluated using a gas chromatograph for the polar gas analysis (GC323, GL Sciences Inc., Tokyo, Japan) according to the published procedure [50].

The membrane performance under the H_2-N_2 (2:1) mixed feed gas flow at p/p_0 (H_2O) = 1.0 was assessed in terms of the separation factor (*SF*):

$$SF = \frac{Y_A / Y_B}{X_A / X_B} \tag{3}$$

where *Y* and *X* are the mass fractions of permeate and feed, respectively and subscripts *A* and *B* denote H_2 and N_2, respectively.

To examine the hydrogen affinity of the AHPCS-derived SiCH organic–inorganic hybrids, the amount of H_2 adsorption onto a thin film of the AHPCS-derived hybrid was measured using a quartz-crystal microbalance (QCM), which is one of the useful methods for detecting in-situ minute mass changes [52]. Commercially available quartz crystal unit (SEN-9E-H-10, Tamadevice Co., Ltd., Kawasaki, Japan) connected with a crystal oscillator circuit (Tamadevice Co. Ltd., Kawasaki, Japan), power supply (GPS-S, GW Instek, Texio Technology Co., Yokohama, Japan) and frequency counter (SC-7205A, UNIVERSALCOUNTER, Iwatsu Electric Co., Ltd., Tokyo, Japan) were used, and the measurement system shown in Figure 1 was set-up at our laboratory.

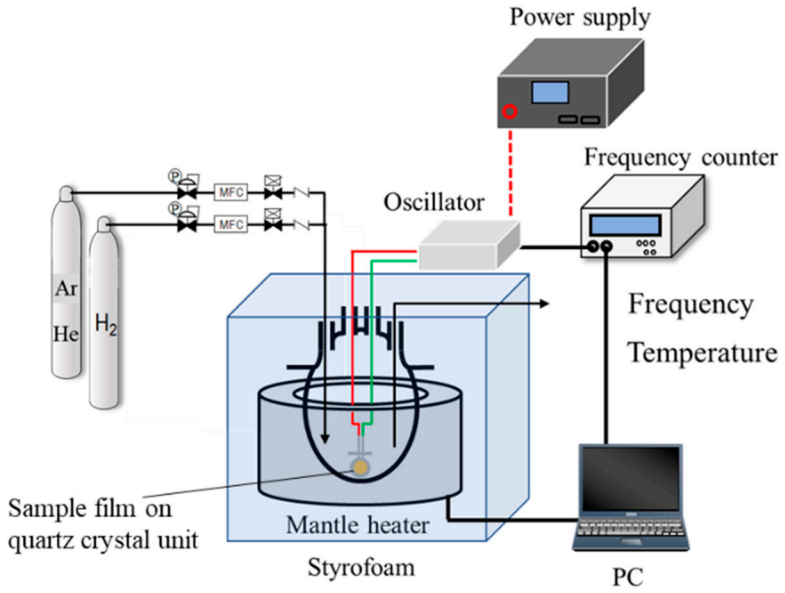

Figure 1. Schematic diagram of the weight change measurement with the quartz crystal microbalance (QCM).

The sample film was formed on the quartz crystal unit surface using the dry xylene solution of as-received AHPCS under the same manner as mentioned for the 300 °C-synthesized membrane. The sample film on the quartz crystal unit was placed in a four-necked round-bottom glass flask. Then, the temperature inside the flask was precisely adjusted at 30 °C (±0.1 °C) by a styrofoam-covered mantle heater operated by the PID control. The sample film was exposed to He atmosphere maintained by a continuous He gas flow at 30 mL min^{-1}. After 15 h, the frequency shift was measured for 90 ks to confirm that the He adsorption reached the equilibrium. Then, the weight change measurement under a H_2 flow (30 mL min^{-1}) was started by switching the feed gas from He to H_2, and the weight change was monitored for an additional 90 ks. The measurement system was controlled by a standard PC with a software (Labview, National Instruments Corp., Austin, TX, USA) for recording the transition of the frequencies corresponding to the mass change.

Conversion from the measured frequency shift Δf (Hz) to the mass change Δm (g) was calculated using the Sauerbrey equation [53],

$$\Delta f = -\frac{2f_0^2}{\sqrt{\mu_q \rho_q}} \frac{\Delta m}{A_e} \quad (4)$$

where, f_0 is the frequency of the quartz crystal prior to a mass change (9.0×10^6 (Hz)), μ_q is the shear modulus of quartz (2.947×10^{13} (g m^{-1} s^{-2})), ρ_q is the density of quartz (2.648 (g cm^{-3})) and A_e is the electrode area (3.93×10^{-5} (m^2)).

3. Results and Discussion

3.1. Heat Treatment Temperatures Selected for Highly Cross-Linked SiCH Organic–Inorganic Hybrid Synthesis

Chemical structure and molecular distribution of the AHPCS are shown in Figures S1 and S2, respectively, in the electric supplementary information (ESI). In this study, the SiCH hybrid polymer of AHPCS was converted into the highly cross-linked SiCH organic–inorganic hybrid as a component of the hydrogen separation membrane. The temperatures for thermal conversion of AHPCS to highly cross-linked SiCH hybrid in this study was selected as 300, 400 and 500 °C based on the results obtained by the TG-MS analyses (Figures S3 and S4 in ESI) as well as FT-IR and Raman spectroscopic analyses for the heat-treated AHPCSs (Figures S5 and S6 in ESI). The thermal behavior of AHPCS has been already studied by several research groups [42,54–58], and the results obtained in this study were well consistent with those previously reported: As shown in Figure S2, as-received AHPCS had a considerable amount of low molecular weight fraction below 1000. TG-MS analyses revealed the thermal decomposition of the low molecular weight fraction proceeded during the first weight loss at 100–300 °C and a second one from 350 to 500 °C by detecting gaseous species assigned to the fragments of carbosilane species (Figures S3 and S4). On the other hand, thermal cross-linking was observed up to 300 °C for the formation of ≡Si-CH_2-CH_2-CH_2-Si≡ and/or ≡Si-CH(CH_3)-CH_2-Si≡ via hydrosilylation between ≡Si-H and ≡Si-CH_2-CH=CH_2 groups in AHPCS, which was identified by the disappearance of the FT-IR absorption band at 1629 cm^{-1} attributed to the C=C bond of the allyl group [55,56] associated with the decrease in the relative FT-IR band intensities assigned to ν(Si-H) at 2123 cm^{-1} and δ(Si-H) at 947 cm^{-1} [55,56] (Figure S5). At 400–700 °C, formation of ≡Si-Si≡ between Si-H and Si-CH_3 groups [42] was suggested by detecting gaseous species at the m/z ratio of 15 assigned to methane (CH_4; Figure S4b). Since the thermal decomposition and cross-linking contentiously proceeded at 300–500 °C, the quantity of organic groups and microporosity of the SiCH hybrid differed depending on the specific heat treatment temperature in this temperature range. On the other hand, the FT-IR spectrum for the 700 °C-heat treated AHPCS revealed that polymer/inorganic silicon carbide conversion almost completed (Figure S5). It should be noted that the samples heat-treated at 300–500 °C were identified as the ternary SiCH Class II hybrid without graphite-like carbon, since the Raman spectra of these samples exhibited several peaks due to the organic groups without those attributed to graphite-like carbon typically detected at 1347.5 and 1596.5 cm^{-1} assigned as D-band (for disordered graphite) and G-band (for the sp2 graphite network), respectively [59,60] (Figure S6). Based on these results, the heat treatment of AHPCS was achieved at 300, 400 and 500 °C for the synthesis of powder and membrane samples.

3.2. Hydrophobicity

The water vapor adsorption–desorption isotherms at 25 °C measured for the powder samples are shown in Figure 2. The AHPCS heat-treated at 300 and 400 °C generated a type III isotherm [61,62], which showed a weak interaction to water molecule. The maximum amount of the water adsorption ((Va(H_2O)) of these samples was below 2 cm^3(STP) g^{-1}. The 500 °C-heat treated AHPCS also showed relatively high hydrophobicity, and the Va(H_2O) remained at 6.3 cm^3 (STP) g^{-1}.

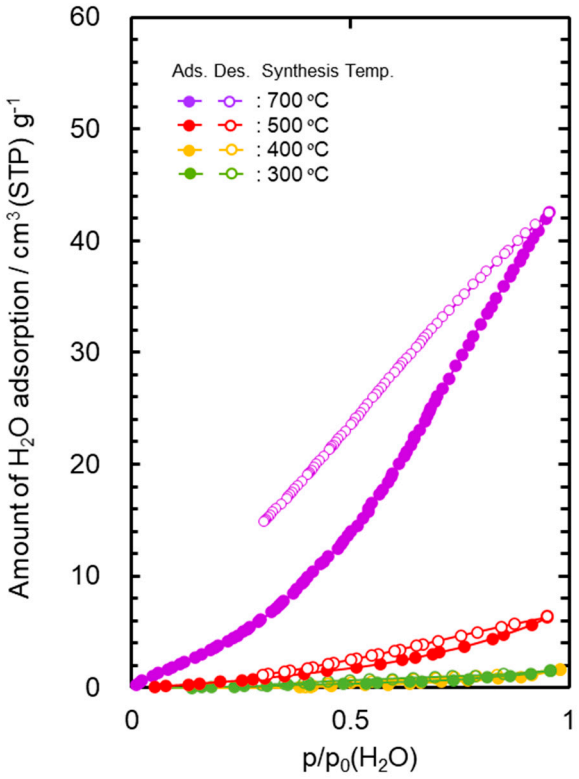

Figure 2. Water vapor adsorption–desorption isotherms at 25 °C for SiCH inorganic–organic hybrid powder samples synthesized by heat treatment of AHPCS at 300–700 °C in Ar.

The Va(H_2O) values evaluated for the AHPCS-derived SiCH were much lower than that of highly hydrophilic mesoporous γ-Al_2O_3 (297 cm^3 (STP) g^{-1}) characterized in our previous study [50].

On the other hand, the 700 °C-heat treated AHPCS presented a type V [61,62]-like isotherm with a large open loop of hysteresis at p/p_0 (H_2O) above 0.3, and the Va(H_2O) reached 42.5 cm^3 (STP) g^{-1}. As shown in Figure S5, the thermal decomposition of the organic groups in AHPCS was almost completed at 700 °C, which led to the analyzed hydrophilic character.

3.3. Properties of SiCH Hybrid/γ-Al_2O_3 Composite Membrane

(1) Structure of the composite membrane

As a typical observation, Figure 3a presents a cross-sectional SEM image of a supported γ-Al_2O_3 membrane after dip coating of the AHPCS xylene solution and subsequent heat treatment at 400 °C under flowing Ar. There was no additional layer on the γ-Al_2O_3 membrane surface. Then, an EDS analysis was performed on the modified membrane. As shown in Figure 3b, the line scan of the EDS mapping for Si derived form AHPCS was detected within the γ-Al_2O_3 membrane having approximately 2.5 μm thickness. Accordingly, the resulting composite membranes in this study were composed of γ-Al_2O_3 with mesopore channels infiltrated by the AHPCS-derived SiCH hybrid.

(2) Gas permeation behaviors under dry condition

Arrhenius plots of He, H_2 and N_2 permeances evaluated for the SiCH hybrid/γ-Al_2O_3 composite membranes synthesized at 300, 400 and 500 °C are shown in Figure 4a–c, respectively. Despite the low permeation temperature of 25 °C, the composite membranes exhibited a relatively high H_2 permeance of 1×10^{-7} to 4×10^{-6} mol m^{-2} s^{-1} Pa^{-1} with a H_2/N_2 permselectivity ($\alpha(H_2/N_2)$) of 9.2–17, apparently higher than that of the theoretical one (3.73) based on the Knudsen's diffusion.

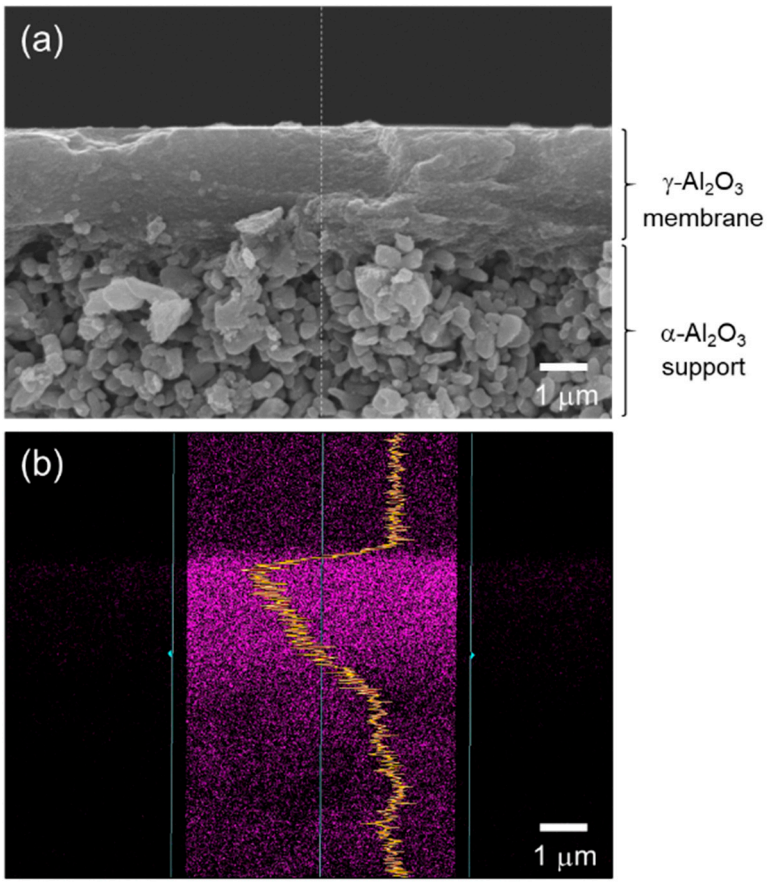

Figure 3. (**a**) A typical cross-sectional SEM image of the γ-Al_2O_3 membrane on a microporous α-Al_2O_3 support after modification with AHPCS and subsequent heat treatment at 400 °C in Ar. (**b**) Line scan of EDS mapping for Si derived from AHPCS detected within the mesoporous γ-Al_2O_3 membrane having a thickness of approximately 2.5 μm.

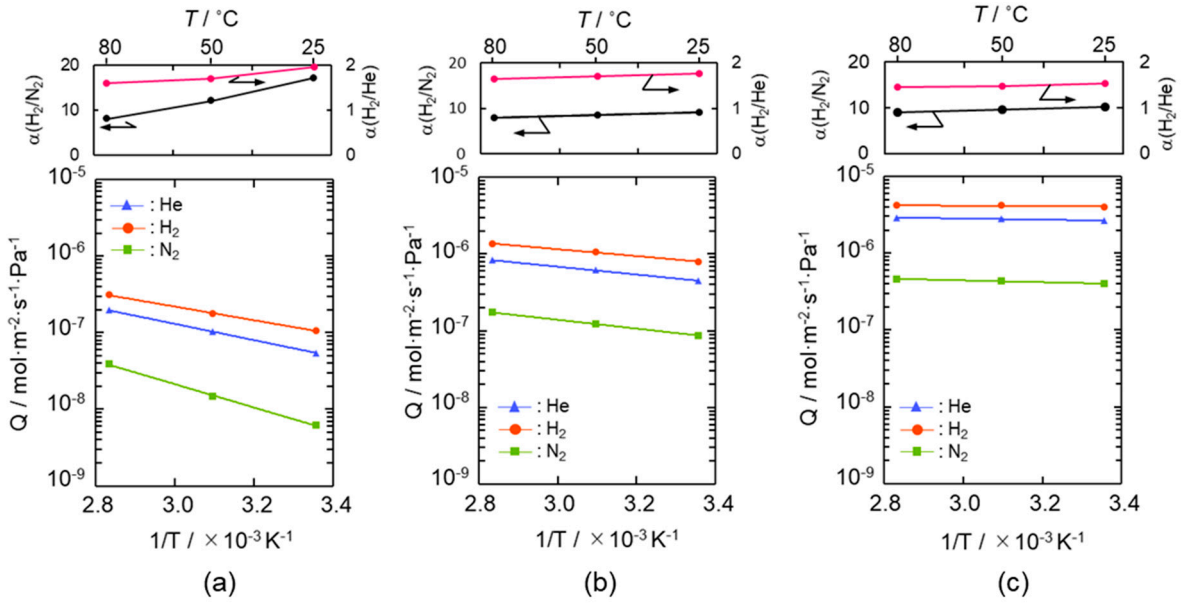

Figure 4. Gas permeation behaviors under dry condition of the supported mesoporous γ-Al_2O_3 membrane after modification with AHPCS and subsequent heat treatment under flowing Ar at (**a**) 300 °C, (**b**) 400 °C and (**c**) 500 °C.

The gas permeation behavior through each composite membrane was similar, and all the gas permeances increased linearly with the permeation temperature and thus followed the Arrhenius law. Since the gas permeations through the supported mesoporous γ-Al_2O_3 membrane exhibited a typical Knudsen's diffusion characteristics in our previous study [50], the gas permeation behaviors observed for the present composite membranes suggested that all the gases permeated through the microporous SiCH hybrid, which filled in the mesopore channels of the γ-Al_2O_3, and the dominant mechanism for the gas permeations was activated diffusion. However, at all permeation temperatures from 25 to 80 °C, the composite membranes exhibited a unique α(H_2/He) of 1.44–1.95, which was higher than the theoretical one (1.41) based on the Knudsen's diffusion.

To highlight this unique gas permeation behavior, the gas permeances measured at 50 °C were characterized and are shown in Figure 5 by plotting the kinetic diameter dependence of the normalized gas (*i*) permeance relative to the He permeance (Q_i/Q_{He}), and compared with the ideal value ($Q_{K,i}/Q_{K,He}$) by the Knudsen model [63,64],

$$\frac{Q_{K,i}}{Q_{K,He}} = \frac{\sqrt{M_{He}}}{\sqrt{M_i}} \quad (5)$$

where M_i and M_{He} are molecular weights of gas-*i* and He, respectively.

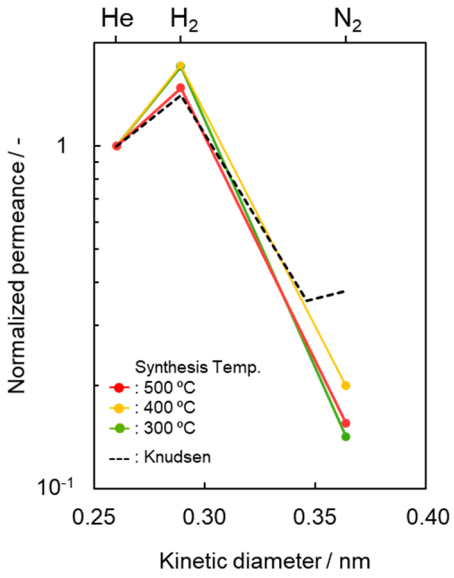

Figure 5. Kinetic diameter dependence of normalized gas permeance based on He permeance (Q_i/Q_{He}) at 50 °C through the SiCH hybrid/γ-Al_2O_3 composite membrane synthesized at different temperatures of 300, 400 and 500 °C. Dotted line indicates predicted values by the Knudsen diffusion model based on He permeance.

The apparent activation energies for He and H_2 permeations were evaluated by the Arrhenius plot (Figure 4) and are listed in Table 1. The apparent activation energy (E_a) for He permeation was 20.3–1.4 kJ mol^{-1}, while that for H_2 permeation was 17.0–0.5 kJ mol^{-1}.

Table 1. Activation energies for He and H_2 permeations through the supported mesoporous γ-Al_2O_3 membrane after modification with AHPCS and subsequent heat treatment at 300–500 °C.

SiCH Hybrid/γ-Al_2O_3 Composite Membrane Synthesis Temp.	Activation Energy (E_a)/kJ mol^{-1}	
	He	H_2
300 °C	20.3	17.0
400 °C	9.8	8.6
500 °C	1.4	0.5

The E_a values for both He and H_2 permeations decreased with the composite membrane synthesis temperature. This tendency was well consistent with the result of TG-MS analyses (Figures S3 and S4) and the gas permeation behaviors (Figure 4): weight loss due to the volatilization of the low molecular weight fraction of as-received AHPCS contentiously proceeded at 300–500 °C (Figure S4), and resulting yields of the SiCH hybrid at 300, 400 and 500 °C were measured to be 87%, 83% and 76%, respectively (Figure S3), while all the gas permeances through the composite membrane increased with the synthesis temperature (Figure 4). Thus, the observed E_a values for He and H_2 permeations could depend on the density of the AHPCS-derived SiCH organic–inorganic hybrid network. However, a unique point was that, regardless of the synthesis temperature, the E_a for H_2 permeation was found to be smaller than that for He permeation, which was a clear contrast to those evaluated for the H_2-selecitve microporous amorphous silica membranes [10,11,65–67]. Then, an attempt was made for study on the hydrogen affinity of the AHPCS-derived SiCH organic–inorganic hybrid: The amount of H_2 adsorption on the AHPCS-derived SiCH film was measured by using a quartz-crystal microbalance (QCM). The SiCH sample film was formed on the quartz crystal unit surface by following the procedure for the composite membrane synthesis at 300 °C (effective film area corresponded to A_e in Equation (2), 3.93×10^{-5} m^2). The sample film was exposed to He atmosphere under the strictly regulated isothermal condition at 30 °C (±0.1 °C) for more than 90 ks. After the He adsorption reached equilibrium, weight gain was monitored by exposing the sample film to H_2 atmosphere under the same isothermal condition. As shown in Figure 6, the weight gain increased with H_2 exposure time and reached 7.14 ng (1.82×10^{-4} g m^{-2}) after the additional 88,130 s. Since the molecular weight of H_2 (2.016) was approximately one-half of He (4.002), the weight gain measured under the H_2 atmosphere revealed preferential adsorption of H_2 relative to He, i.e., existence of H_2 affinity of the AHPCS-derived SiCH organic–inorganic hybrid, which might contribute to the experimentally observed unique $\alpha(H_2/He) >$ 1.41 and high H_2 permeances (10^{-7}–10^{-6} mol m^{-2} s^{-1} Pa^{-1} order at 25–80 °C).

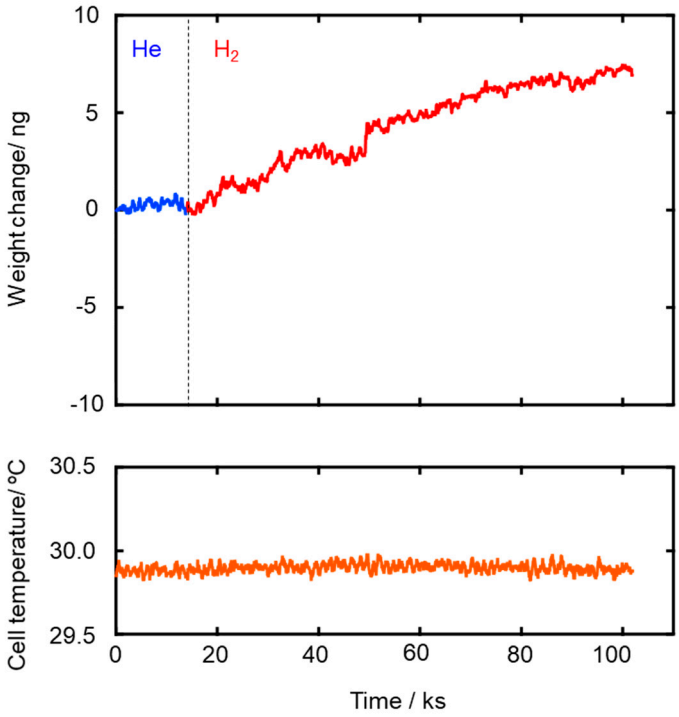

Figure 6. Weight gain measured at 30 °C for H_2 adsorption to the sample film of the SiCH organic–inorganic hybrid prepared by 300 °C-heat treatment in Ar.

(3) Gas permeation behaviors under the wet condition

For study on the potential application to the solar hydrogen production system, the gas permeation measurement was performed on the composite membranes by using a mixed H_2-N_2 feed gas in the molar ratio 2:1 under dry and saturated water vapor partial pressure (p/p_0 (H_2O) = 1) at 50 °C. The results are summarized and shown in Figure 7. The composite membranes were found to be water vapor permeable and the permeance was measured to be 2.7–3.8 × 10^{-7} mol m^{-2} s^{-1} Pa^{-1}.

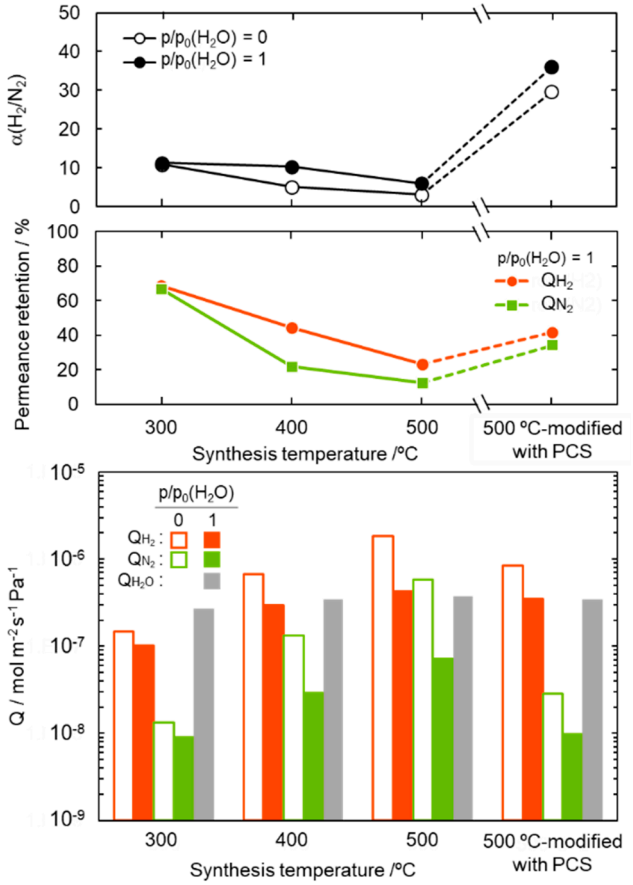

Figure 7. Gas permeation properties under the dry ($p/p_0(H_2O)$ = 0) and wet ($p/p_0(H_2O)$ = 1) condition at 50 °C, and water vapor permeation properties at $p/p_0(H_2O)$ = 1 at 50 °C evaluated for SiCH hybrid/γ-Al_2O_3 composite membranes synthesized at different temperatures of 300, 400 and 500 °C, and the 500 °C-synthesized membrane further modified with PCS by the melt impregnation at 120 °C [50].

The $\alpha(H_2/N_2)$ of the composite membranes was 6.0–11.3, and regardless of the synthesis temperature, there was no significant degradation under the highly humid condition at 50 °C. The 300 °C-synthesized composite membrane kept relatively high gas permeances. The retentions evaluated for the H_2 and N_2 permeances under the p/p_0 (H_2O) = 1 at 50 °C were 69 and 67%, respectively. However, with increasing synthesis temperature, the permeance retention of both H_2 and N_2 decreased, in other words, the hydrophobicity in terms of stable gas permeation property degraded with the synthesis temperature. This degradation tendency is consistent with the temperature dependence of the SiCH hybrid polymer/highly cross-linked SiCH hybrid conversion yield as described above, and thus is related to the quantity of organic groups remained in the SiCH hybrid and the microporosity or volume of the SiCH hybrid, which infiltrated the mesopore channels of the composite membrane.

Then, the 500 °C-synthesized composite membrane was further modified with polycarbosilane (PCS) by the 120 °C-melt impregnation established by our previous study [50]. As shown in Figure 7, under the

dry condition at 50 °C, the PCS-modified composite membrane showed a relatively high H_2 permeance of 8.4×10^{-7} mol m^{-2} s^{-1} Pa^{-1} with a significantly improved $\alpha(H_2/N_2)$ of 29.6. Moreover, under the p/p_0 (H_2O) = 1 at 50 °C, the PCS-modification successfully improved the membrane performance: H_2 permeance and $\alpha(H_2/N_2)$ were measured to be 3.5×10^{-7} mol m^{-2} s^{-1} Pa^{-1} and 36, respectively.

Gas permeation properties under the wet condition at 50 °C of the composite membranes were also assessed by cyclic gas permeance measurements under $p/p_0(H_2O)$ ranging from 0.1 to 1.0 and compared with those of the supported mesoporous γ-Al_2O_3 membrane itself. As shown in Figure 8a, H_2 and N_2 permeances through the supported mesoporous γ-Al_2O_3 membrane drastically decreased above $p/p_0(H_2O)$ = 0.74. This degradation is due to the highly hydrophilic property of γ-Al_2O_3, which leads to the blockage of the gas permeable mesopore channels by adsorption and subsequent condensation of water molecules as the permeate [50]. On the other hand, the 300 °C-synthesized composite membrane exhibited stable gas permeations at all the $p/p_0(H_2O)$ up to 1.0 (Figure 8b). A slight decrease in the gas permeances at $p/p_0(H_2O) > 0.74$ was due to the pressure-drop caused by the water vapor condensation within the mesopore channels of hydrophilic γ-Al_2O_3 partly remained without surface modification with the AHPCS-derived hydrophobic hybrid. The 500 °C-synthesized composite membrane also showed the decreasing tendency in gas permeances, however further modification with PCS successfully improved the membrane performance at the final gas permeation measurement under the saturated humidity at 50 °C: H_2 permeance remained at 10^{-7} mol m^{-2} s^{-1} Pa^{-1} order with $\alpha(H_2/N_2) > 30$ under (Figure 8c), and the resulting separation factor (SF) evaluated based on the gas permeation data shown in Table 2 was found as 26.

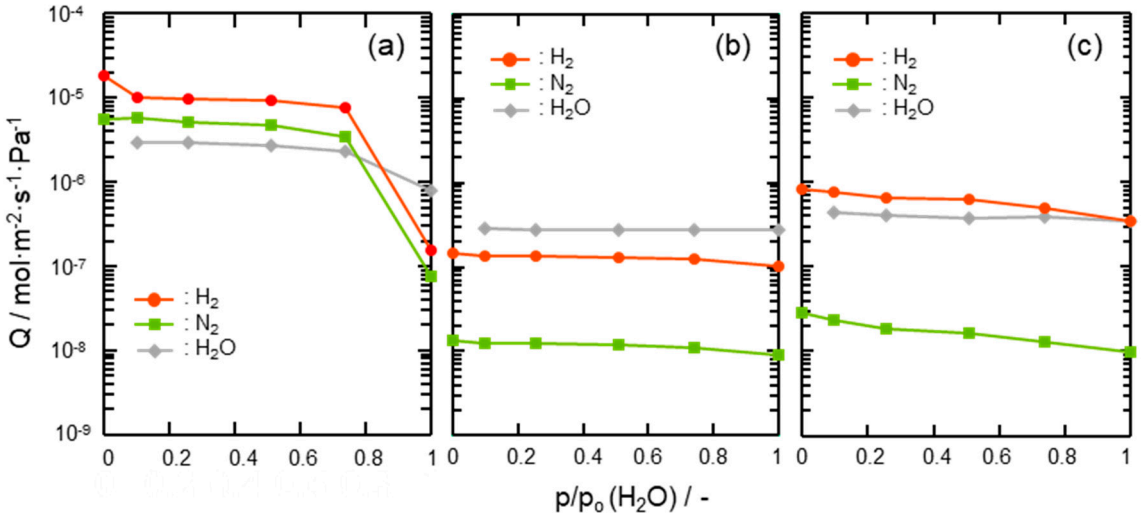

Figure 8. Results of cyclic gas permeation measurements at 50 °C under $p/p_0(H_2O)$ = 0–1.0 using the H_2-N_2 (2:1) mixed feed gas evaluated for (**a**) a supported mesoporous γ-Al_2O_3 membrane, (**b**) a 300 °C-synthesized SiCH hybrid/γ-Al_2O_3 composite membrane and (**c**) a 500 °C-synthesized composite membrane further modified with PCS.

Table 2. Gas permeation data of 500 °C-synthesized membrane further modified with PCS measured at 50 °C under p/p_0 (H_2O) =1.0 using a H_2-N_2 (2:1) mixed feed gas.

Feed Side		Permeate Side				Separation Factor (SF)
Flow Rate, $V_F/\times 10^{-5}$ mol s^{-1}		Flow Rate, $V/\times 10^{-5}$ mol s^{-1}		Flux, $J/\times 10^{-5}$ mol m^{-2} s^{-1}		
$V_{F,H2}$	$V_{F,N2}$	V_{H2}	V_{N2}	J_{H2}	J_{N2}	
14.7	7.4	2.2	0.043	2971.8	56.6	26

Moreover, the polymer-derived SiCH organic–inorganic hybrid investigated in this study showed sufficient stability under the present high humidity conditions at 50 °C: Figure 9 presents the top

surface view of the 500 °C-synthesized composite membrane modified with PCS before and after the cyclic gas permeation measurements under $p/p_0(H_2O)$ up to 1.0 at 50 °C. Compared with the surface of the as-synthesized mesoporous γ-Al_2O_3 membrane over an α-Al_2O_3 porous support (Figure 9a), the composite membrane exhibited a smooth surface (Figure 9b) and kept the surface without structural degradation after the cyclic gas permeation measurements (Figure 9c). These results revealed that, in addition to hydrogen permselectivity, the modification with the polymer-derived SiCH organic–inorganic hybrid investigated in this study greatly improved the hydrophobicity in terms of stable gas permeations under the saturated water vapor partial pressure at 50 °C.

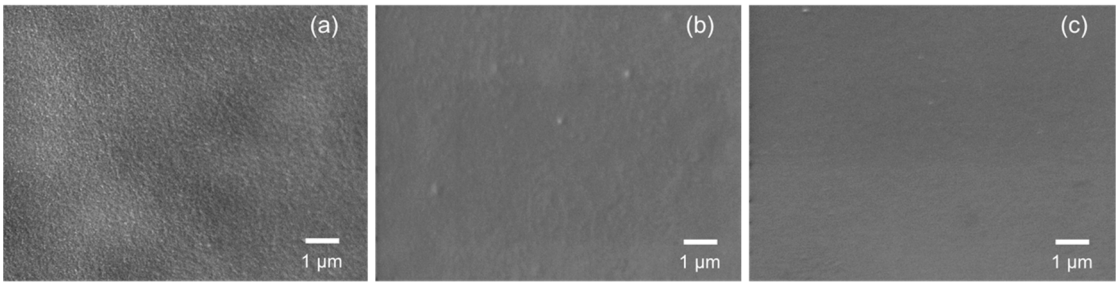

Figure 9. SEM images of the top surface view of an (**a**) as-synthesized mesoporous γ-Al_2O_3 layer and 500 °C-synthesized membrane further modified with PCS (**b**) before and (**c**) after gas permeation measurements under $p/p_0(H_2O)$ up to 1 at 50 °C.

The H_2-permselectivities of the composite membrane measured in this study were briefly compared with those recently reported for other membranes composed of various materials systems, and their H_2 permeation data with $\alpha(H_2/X)$ (X = N_2 (0.364 nm) [51] or O_2 (0.346 nm) [51]) measured under the dry condition at $T \leq 50$ °C are listed in Table 3 [18,68–78]. Among them, novel ultrathin (9 nm thickness) graphene oxide membrane formed on an anodic oxidized alumina support (#09) exhibited a H_2 permeance of approximately 1×10^{-7} mol m^{-2} s^{-1} Pa^{-1} with $\alpha(H_2/N_2)$ of 900 at 20 °C [75,76]. The zeolite imidazolate framework (ZIF) nanosheet membrane (#08) also showed H_2 permeance of 2.04×10^{-7} mol m^{-2} s^{-1} Pa^{-1} with high $\alpha(H_2/N_2)$ of 66.6 at 30 °C [73,74]. Among other practical membranes, SiO_2-based organic–inorganic hybrid membrane (#03) showed the highest H_2 permeance of 10^{-6} mol m^{-2} s^{-1} Pa^{-1} order, while the $\alpha(H_2/N_2)$ remained at 12 [68]. On the other hand, zeolite/CMC (carbon molecular sieve) composite membranes (#04, #05) showed a high $\alpha(H_2/N_2)$ of 61-100.2, however the H_2 permeance at 30 °C was 10^{-9}–10^{-8} mol m^{-2} s^{-1} Pa^{-1} order [69,70].

As shown in Figures 4 and 5, in addition to the H_2/N_2 selectivity, the present composite membranes exhibited unique H_2/He selectivity due to the H_2 affinity of the AHPCS-derived highly cross-linked SiCH organic–inorganic hybrid in the composite membrane (Figure 6). This unique H_2 preferential permeation property contributed to relatively high H_2 permeance of 8.4×10^{-7} mol m^{-2} s^{-1} Pa^{-1} with $\alpha(H_2/N_2)$ of 29.6.

For the application of the purification of solar hydrogen, the long-term stability and robustness of H_2-selecitve membranes under the humid condition at around 50 °C are practical issues for us to pursue. In this context, there are few reports as mentioned above, and Oyama et al. reported [18] their pioneering study on the stability of PFDA-based liquid membrane (#06 in Table 3) under the humid condition (10 mol%) at 30 °C as a simulated condition for the purification of solar hydrogen, and they confirmed its stability for up to 48 h. The stabilities of the composited membranes characterized by the primary accelerated degradation test (Figures 7–9) were compatible with that of the supported liquid membrane (#06 in Table 3) [18]. Under the scheme of the current NEDO R&D "Artificial Photosynthesis" Project, we plan to conduct the long-term stability test for the composite membranes by using a H_2-O_2 (2:1) mixed feed gas as a simulated syngas at the project facility with safety measures against explosion.

Table 3. H_2-permselectivities of composite membrane in this study and those of other membranes evaluated at $T \leq 50$ °C under the dry condition.

No.	Membranes	Temp./°C	H_2 Permeance /mol m^{-2} s^{-1} Pa^{-1}	H_2/X Selectivity $\alpha(H_2/X)$	X	Ref.
#01	500 °C modified with PCS, Dry	50	8.4×10^{-7}	29.6	N_2	This study
	Wet, $p/p_0(H_2O) = 1.0$	50	3.5×10^{-7}	36.1	N_2	
#02	SiO_2-based organic–inorganic hybrid (BTESE)	40	7.66×10^{-7}	−20	N_2	[68]
#03	SiO_2-based organic–inorganic hybrid (BTESM)	50	1.79×10^{-6}	12	N_2	
#04	zeolite-β/CMS	30	2.64×10^{-9}	97	N_2	[69,70]
		30	1.95×10^{-8}	67.3	N_2	
#05	zeolite-Y/CMS	30	2.77×10^{-9}	100.2	N_2	
		30	1.96×10^{-8}	61	N_2	
#06	PFDA-based liquid membrane	30	2.4×10^{-9}	10	O_2	[18]
#07	graphene nanosheet	RT	5.9×10^{-7}	16.5	N_2	[71,72]
#08	ZIF nanosheet membrane	30	2.04×10^{-7}	66.55	N_2	[73,74]
#09	ultrathin graphene oxide	20	-1×10^{-7}	−900	N_2	[75,76]
#10	microporous polymer (PIM-EA(H_2)-TB)	30	(1.7×10^{-12}) *	22	N_2	[77]
#11	microporous polymer (PIM-Trip(Me_2)-TB)	25	(1.8×10^{-12}) *	21.4	N_2	[78]

*: H_2 permeability/mol m^{-1} s^{-1} Pa^{-1}.

4. Conclusions

In this study, AHPCS was converted to highly cross-linked ternary SiCH organic–inorganic hybrid compounds by heat treatment at 300–500 °C under Ar atmosphere. The water vapor adsorption–desorption isotherm measurement revealed that the AHPCS-derived highly cross-linked SiCH hybrids exhibited excellent hydrophobicity, and the maximum amount of water vapor adsorption at 25 °C was 1.5–6.3 cm^3 (STP) g^{-1}.

Aiming to develop H_2-selective membranes for the application of the novel solar hydrogen production system, a supported mesoporous γ-Al_2O_3 membrane with a thickness of about 2.5 μm was modified with AHPCS xylene solution and subsequently heat-treated at 300–500 °C under Ar atmosphere. SEM observation revealed that the mesoporous channels of the γ-Al_2O_3 membrane were coated by the AHPCS-derived SiCH to afford a SiCH hybrid/γ-Al_2O_3 composite membrane. Even at a low temperature of 25 °C, the composite membranes exhibited a high H_2 permeance of 1×10^{-7} to 4×10^{-6} mol m^{-2} s^{-1} Pa^{-1} and a $\alpha(H_2/N_2)$ of 9.2–17 together with a unique $\alpha(H_2/He)$ of 1.44–1.95.

The apparent activation energy for the H_2 permeation at 25–80 °C was 17.0–0.5 kJ mol^{-1} and found to be smaller than that for He (20.3–1.4 kJ mol^{-1}). Moreover, the measurement of H_2 adsorption on an AHPCS-derived SiCH film by using a QCM revealed preferential H_2 adsorption at 30 °C. These results strongly indicate a significant H_2 affinity of the AHPCS-derived SiCH organic–inorganic hybrid, which contributes to the experimentally observed unique $\alpha(H_2/He)$ and the high H_2 permeance at 25–80 °C.

As a simulated wet condition for the purification of solar hydrogen, the gas permeation measurement under saturated water vapor partial pressure at 50 °C was performed on the composite membranes by using a mixed H_2-N_2 feed gas in the molar ratio 2:1. The 300–500 °C synthesized composite membranes exhibited a relatively high H_2 permeance of $1.0–4.3 \times 10^{-7}$ mol m^{-2} s^{-1} Pa^{-1} with a $\alpha(H_2/N_2)$ of 6.0–11.3. Further modification by the 120 °C-melt impregnation of PCS successfully improved the H_2-permselectivity of the 500 °C synthesized composite membrane by maintaining the H_2

permeance combination with improved $\alpha(H_2/N_2)$ as 3.5×10^{-7} mol m^{-2} s^{-1} Pa^{-1} and 36. These results clearly revealed a promising potential of polymer-derived SiCH organic–inorganic hybrids to develop advanced H_2 selective membranes applicable to novel solar hydrogen production systems.

Supplementary Materials: The following are available online at http://www.mdpi.com/2077-0375/10/10/258/s1, **Figure S1:** Structure of commercially available allyl-hydrido-polycarbosilane (AHPCS), **Figure S2:** Molecular weight distribution of as-received AHPCS, **Figure S3:** Thermal behavior of as-received AHPCS. (a) TG curve and total ion current chromatogram (TICC) under flowing He, and typical mass spectra recorded during (b) the first weight loss from100 to 250 °C and (c) the second weight loss from 350 to 500 °C, **Figure S4:** Continuous in-situ monitoring of gaseous species by mass spectrometry: (a) Fragments derived from low molecular weight fraction of as-received AHPCS during the first weight loss from 100 to 300 °C and the second one from 350 to 500 °C and (b) methane (CH_4) at 400 to 700 °C. (c) Fragments suggested for gaseous spices derived from low molecular weight fraction of as-received AHPCS (Equation (1)), m/z = 42 ($(CH_2)_3$) from AHPCS after cross-linking via hydrosilylation between ≡Si-H and CH_2=CH-CH_2-Si≡ (Equations (2) and (3)) and m/z = 15 (CH_4) due to the thermal crosslinking between ≡Si-H and ≡Si-CH_3 groups to afford ≡Si-Si≡ above 350 °C (Equation (4)) [42], **Figure S5:** FT-IR spectra for as-received AHPCS and those after heat treatment at 300 to 700 °C in Ar, **Figure S6:** Raman spectra for as-received and those AHPCS after heat treatment at 300 to 500 °C in Ar. Spectra indicated the heat-treated samples were free from graphite-like carbon typically detected at 1347.5 and 1596.5 cm^{-1} attributed to the D-band (for disordered graphite) and G-band (for the sp2 graphite network), respectively [59,60].

Author Contributions: Conceptualization, M.K. (Miwako Kubo) and Y.I.; methodology, Y.D. and E.I.; investigation, R.M., M.K. (Misako Kojima) and K.N.; Formal analysis, S.H.; writing—original draft preparation, M.K. (Miwako Kubo) and Y.I.; writing—review and editing, S.B. and R.R.; visualization, supervision and funding acquisition, Y.I. All authors have read and agreed to the published version of the manuscript.

Funding: This work was in part supported by "Research Project for Future Development: Artificial Photosynthetic Chemical Process (ARPChem)" (METI/NEDO, Japan: 2012-2022). Samuel Bernard and Yuji Iwamoto would like to thank CNRS who financially supported present work via the International Research Project (IRP) 'Ceramics materials for societal challenges'.

Conflicts of Interest: The authors declare no conflict of interest.

Nomenclature

A	membrane area, m^2
A_e	electrode area, m^2
E_a	activation energy, kJ mol^{-1}
Df	measured frequency shift, Hz
f_0	frequency of quartz crystal prior to a mass change, Hz
Δm	mass change, g
M_i	molecular weights of gas-*i*, kg mol^{-1}
p/p$_0$ (H_2O)	relative pressure of water vapor, dimensionless
p_H	pressures of gas feed side, Pa
p_L	pressures of gas permeate side, Pa
Q_i	permeance of gas-*i*, mol m^{-2} s^{-1} Pa^{-1}
$Q_{K,i}$	Knudsen permeance of gas-*i*, mol m^{-2} s^{-1} Pa^{-1}
V	permeate molar flow rate, mol s^{-1}
Va(H_2O)	maximum amount of water adsorption, cm^3(STP) g^{-1}

Greek Symbols

α	permselectivity, dimensionless
ρ_q	shear modulus of quartz, g m^{-1} s^{-2}
μ_q	density of quartz, g cm^{-3}

Abbreviations

AHPCS	allyl-hydro-polycarbosilane
BTESE	1,2-bis(triethoxysilyl)ethane
BTESM	bis(triethoxysilyl)methane
CMS	carbon molecular sieve
EA	ethanoanthracene
MOF	metal organic framework
PCS	polycarbosilane
PDCs	Polymer-Derived Ceramics
PDS	polydimethylsilane
PEC	photoelectrochemical
PFDA	1H,1H,2H,2H-perfluorodecyl acrylate
PIM	polymers of intrinsic microporosity
QCM	quartz-crystal microbalance
SF	separation factor
STP	standard temperature and pressure (273.15 K and 101.30 kPa)
THF	tetrahydrofuran
TB	6H,12H-5,11-methanodibenzo[b,f][1,5]diazocine (Tröger's base)
Trip	triptycene
ZIF	zeolite imidazolate framework

References

1. Ogden, J.M.; Williams, R.H.; Larson, E.D. Societal lifecycle costs of cars with alternative fuels/engines. *Energy Policy* **2004**, *32*, 7–27. [CrossRef]
2. Maeda, K.; Domen, K. New non-oxide photocatalysts designed for overall water splitting under visible light. *J. Phys. Chem. C* **2007**, *111*, 7851–7861. [CrossRef]
3. Wang, Q.; Hisatomi, T.; Jia, Q.; Tokudome, H.; Zhong, M.; Wang, C.; Pan, Z.; Takata, T.; Nakabayashi, M.; Shibata, N. Scalable water splitting on particulate photocatalyst sheets with a solar-to-hydrogen energy conversion efficiency exceeding 1%. *Nat. Mater.* **2016**, *15*, 611–615. [CrossRef] [PubMed]
4. Goto, Y.; Hisatomi, T.; Wang, Q.; Higashi, T.; Ishikiriyama, K.; Maeda, T.; Sakata, Y.; Okunaka, S.; Tokudome, H.; Katayama, M.; et al. A Particulate Photocatalyst Water-Splitting Panel for Large-Scale Solar Hydrogen Generation. *Joule* **2018**, *2*, 509–520. [CrossRef]
5. Yamada, T.; Domen, K. Development of Sunlight Driven Water Splitting Devices towards Future Artificial Photosynthetic Industry. *ChemEngineering* **2018**, *2*, 36. [CrossRef]
6. Development of Basic Chemical Processes for Carbon Dioxide as Raw Material. Available online: www.nedo.go.jp/activities/EV_00296.html (accessed on 2 August 2020).
7. Yagyu, S.; Matsui, H.; Matsuda, T.; Yasumoto, H. *Studies of Explosive Characteristics of Hydrogen (1st Report)*; RIIS-RR-18-1; Ministry of Labour, the Research Institute of Industrial Safety, 1969. Available online: www.jniosh.johas.go.jp/publication/doc/rr/RR-18-1.pdf (accessed on 2 August 2020).
8. Tanaka, K.; Sakata, Y. Present and Future Prospects of Hydrogen Production Process Constructed by the Combination of Photocatalytic H_2O Splitting and Membrane Separation Process. *Membrane* **2011**, *36*, 113–121. [CrossRef]
9. Oyama, S.T.; Stagg-Williams, S.M. *Inorganic, Polymeric and Composite Membranes: Structure, Function and Other Correlations*; Elsevier: Amsterdam, The Netherlands, 2011.
10. Mise, Y.; Ahn, S.J.; Takagaki, A.; Kikuchi, R.; Oyama, S.T. Fabrication and evaluation of trimethylmethoxysilane (TMMOS)-derived membranes for gas separation. *Membranes* **2019**, *9*, 123. [CrossRef]
11. Kato, H.; Lundin, S.-T.B.; Ahn, S.-J.; Takagaki, A.; Kikuchi, R.; Oyama, S.T. Gas Separation Silica Membranes Prepared by Chemical Vapor Deposition of Methyl-Substituted Silanes. *Membranes* **2019**, *9*, 144. [CrossRef]
12. Ted Oyama, S.; Aono, H.; Takagaki, A.; Sugawara, T.; Kikuchi, R. Synthesis of silica membranes by chemical vapor deposition using a dimethyldimethoxysilane precursor. *Membranes* **2020**, *10*, 50. [CrossRef]
13. Yun, S.; Ted Oyama, S. Correlations in palladium membranes for hydrogen separation: A review. *J. Membr. Sci.* **2011**, *375*, 28–45. [CrossRef]

14. Liguori, S.; Iulianelli, A.; Dalena, F.; Pinacci, P.; Drago, F.; Broglia, M.; Huang, Y.; Basile, A. Performance and long-term stability of Pd/PSS and Pd/Al_2O_3 membranes for hydrogen separation. *Membranes* **2014**, *4*, 143–162. [CrossRef] [PubMed]
15. Alique, D.; Martinez-Diaz, D.; Sanz, R.; Calles, J.A. Review of supported Pd-based membranes preparation by electroless plating for ultra-pure hydrogen production. *Membranes* **2018**, *8*, 5. [CrossRef] [PubMed]
16. Castro-Dominguez, B.; Leelachaikul, P.; Takagaki, A.; Sugawara, T.; Kikuchi, R.; Oyama, S.T. Supported perfluorotributylamine liquid membrane for H_2/O_2 separation. *J. Memb. Sci.* **2013**, *448*, 262–269. [CrossRef]
17. Leelachaikul, P.; Castro-Dominguez, B.; Takagaki, A.; Sugawara, T.; Kikuchi, R.; Oyama, S.T. Perfluorooctanol-based liquid membranes for H_2/O_2 separation. *Sep. Purif. Technol.* **2014**, *122*, 431–439. [CrossRef]
18. Yamaguchi, T.; Takagaki, A.; Sugawara, T.; Kikuchi, R.; Oyama, S.T. Supported fluorocarbon liquid membranes for hydrogen/oxygen separation. *J. Membr. Sci.* **2016**, *520*, 272–280. [CrossRef]
19. Burneau, A.; Lepage, J.; Maurice, G. Porous silica-water interactions. I. Structural and dimensional changes induced by water adsorption. *J. Non-Cryst. Solids* **1997**, *217*, 1–10. [CrossRef]
20. Tsuru, T.; Hino, T.; Yoshioka, T.; Asaeda, M. Permporometry characterization of microporous ceramic membranes. *J. Membr. Sci.* **2001**, *186*, 257–265. [CrossRef]
21. Díaz, U.; Corma, A. Organic-Inorganic Hybrid Materials: Multi-Functional Solids for Multi-Step Reaction Processes. *Chem.-A Eur. J.* **2018**, *24*, 3944–3958. [CrossRef]
22. Mir, S.H.; Nagahara, L.A.; Thundat, T.; Mokarian-Tabari, P.; Furukawa, H.; Khosla, A. Review—Organic-Inorganic Hybrid Functional Materials: An Integrated Platform for Applied Technologies. *J. Electrochem. Soc.* **2018**, *165*, B3137–B3156. [CrossRef]
23. Bill, J.; Aldinger, F. Precursor-derived Covalent Ceramics. *Adv. Mater.* **1995**, *7*, 775–787. [CrossRef]
24. Riedel, R. Advanced Ceramics from Inorganic Polymers. In *Materials Science and Technology*; Brook, R.J., Ed.; Wiley-VCH: Weinheim, Germany, 1996; Volume 17B, pp. 1–50.
25. Judeinstein, P.; Sanchez, C. Hybrid organic–inorganic materials: A land of multidisciplinarity. *J. Mater. Chem.* **1996**, *6*, 511–525. [CrossRef]
26. Yajima, S.; Hayashi, J.; Omori, M. Continuous silicon carbide fiber of high tensile strength. *Chem. Lett.* **1975**, *4*, 931–934. [CrossRef]
27. Yajima, S.; Okamura, K.; Hayashi, J.; Omori, M. Synthesis of Continuous SiC Fibers with High Tensile Strength. *J. Am. Ceram. Soc.* **1976**, *59*, 324–327. [CrossRef]
28. Colombo, P.; Mera, G.; Riedel, R.; Sorarù, G.D. Polymer-derived ceramics: 40 Years of research and innovation in advanced ceramics. *J. Am. Ceram. Soc.* **2010**, *93*, 1805–1837. [CrossRef]
29. Hotza, D.; Di Luccio, M.; Wilhelm, M.; Iwamoto, Y.; Bernard, S.; Diniz da Costa, J.C. Silicon carbide filters and porous membranes: A review of processing, properties, performance and application. *J. Membr. Sci.* **2020**, *610*, 118193. [CrossRef]
30. Lee, L.-L.; Tsai, D.-S. A Hydrogen-Permselective Silicon Oxycarbide Membrane Derived from Polydimethylsilane. *J. Am. Ceram. Soc.* **1999**, *82*, 2796–2800. [CrossRef]
31. Shelekhin, A.B.; Grosgogeat, E.J.; Hwang, S.T. Gas separation properties of a new polymer/inorganic composite membrane. *J. Membr. Sci.* **1992**, *66*, 129–141. [CrossRef]
32. Kusakabe, K.; Yan Li, Z.; Maeda, H.; Morooka, S. Preparation of supported composite membrane by pyrolysis of polycarbosilane for gas separation at high temperature. *J. Membr. Sci.* **1995**, *103*, 175–180. [CrossRef]
33. Li, Z.; Kusakabe, K.; Morooka, S. Preparation of thermostable amorphous Si-C-O membrane and its application to gas separation at elevated temperature. *J. Membr. Sci.* **1996**, *118*, 159–168. [CrossRef]
34. Li, Z.; Kusakabe, K.; Morooka, S. Pore Structure and Permeance of Amorphous Si-C-O Membranes with High Durability at Elevated Temperature. *Sep. Sci. Technol.* **1997**, *32*, 1233–1254. [CrossRef]
35. Suda, H.; Yamauchi, H.; Uchimaru, Y.; Fujiwara, I.; Haraya, K. Preparation and gas permeation properties of silicon carbide-based inorganic membranes for hydrogen separation. *Desalination* **2006**, *193*, 252–255. [CrossRef]
36. Nagano, T.; Sato, K.; Saitoh, T.; Iwamoto, Y. Gas permeation properties of amorphous SiC membranes synthesized from polycarbosilane without oxygen-curing process. *J. Ceram. Soc. Jpn.* **2006**, *114*, 533–538. [CrossRef]
37. Takeyama, A.; Sugimoto, M.; Yoshikawa, M. Gas permeation property of SiC membrane using curing of polymer precursor film by electron beam irradiation in helium atmosphere. *Mater. Trans.* **2011**, *52*, 1276–1280. [CrossRef]

38. Elyassi, B.; Deng, W.; Sahimi, M.; Tsotsis, T.T. On the use of porous and nonporous fillers in the fabrication of silicon carbide membranes. *Ind. Eng. Chem. Res.* **2013**, *52*, 10269–10275. [CrossRef]
39. Dabir, S.; Deng, W.; Sahimi, M.; Tsotsis, T. Fabrication of silicon carbide membranes on highly permeable supports. *J. Membr. Sci.* **2017**, *537*, 239–247. [CrossRef]
40. Ciora, R.J.; Fayyaz, B.; Liu, P.K.T.; Suwanmethanond, V.; Mallada, R.; Sahimi, M.; Tsotsis, T.T. Preparation and reactive applications of nanoporous silicon carbide membranes. *Chem. Eng. Sci.* **2004**, *59*, 4957–4965. [CrossRef]
41. Sandra, F.; Ballestero, A.; NGuyen, V.L.; Tsampas, M.N.; Vernoux, P.; Balan, C.; Iwamoto, Y.; Demirci, U.B.; Miele, P.; Bernard, S. Silicon carbide-based membranes with high soot particle filtration efficiency, durability and catalytic activity for CO/HC oxidation and soot combustion. *J. Membr. Sci.* **2016**, *501*, 79–92. [CrossRef]
42. Wang, Q.; Yokoji, M.; Nagasawa, H.; Yu, L.; Kanezashi, M.; Tsuru, T. Microstructure evolution and enhanced permeation of SiC membranes derived from allylhydridopolycarbosilane. *J. Membr. Sci.* **2020**, 118392. [CrossRef]
43. Interrante, L.V.; Shen, Q. Polycarbosilanes. In *Silicon-Containing Polymers*; Jones, R.G., Ando, W., Chojnowski, J., Eds.; Kluwer Academic Publisher: Dordrecht, The Netherlands, 2000; pp. 247–321.
44. Matsumoto, K. Polycarbosilanes. In *Encyclopedia of Polymer Science and Technology*; Mark, H.F., Ed.; John Wiley & Sons: New York, NY, USA, 2003; Volume 7, pp. 426–438.
45. Matsumoto, K.; Endo, T. Synthesis and ring-opening polymerization of functional silacyclobutane derivatives and their application to lithium ion batteries. *Macromol. Symp.* **2015**, *349*, 21–28. [CrossRef]
46. Yajima, S.; Shishido, T.; Okamira, K. SiC Bodies Sintered with Three-Dimensional Cross-Linked Polycarbosilane. *Am. Ceram. Soc. Bull.* **1977**, *56*, 1060–1063.
47. Kim, Y.-W.; Lee, J.-G. Effect of polycarbosilane addition on mechanical properties of hot-pressed silicon carbide. *J. Mater. Sci.* **1992**, *27*, 4746–4750. [CrossRef]
48. Czubarow, P.; Seyferth, D. Application of poly(methylsilane) and Nicalon® polycarbosilane precursors as binders for metal/ceramic powders in preparation of functionally graded materials. *J. Mater. Sci.* **1997**, *32*, 2121–2130. [CrossRef]
49. Sawai, Y.; Iwamoto, Y.; Okuzaki, S.; Yasutomi, Y.; Kikuta, K.; Hirano, S. Synthesis of Silicon Carbide Ceramics Using Chemically Modified Polycarbosilanes as a Compaction Binder. *J. Am. Ceram. Soc.* **1999**, *82*, 2121–2125. [CrossRef]
50. Kubo, M.; Kojima, M.; Mano, R.; Daiko, Y.; Honda, S.; Iwamoto, Y. A hydrostable mesoporous γ-Al_2O_3 membrane modified with Si–C–H organic-inorganic hybrid derived from polycarbosilane. *J. Membr. Sci.* **2020**, *598*, 117799. [CrossRef]
51. Breck, D.W. *Zeolite Molecular Sieves: Structure, Chemistry, and Use*; John Wiley & Sons: New York, NY, USA, 1974; ISBN 978-0471099857.
52. Buttry, D.A.; Ward, M.D. Measurement of Interfaclal Processes at Electrode Surfaces with the Electrochemical Quartz Crystal Microbalance. *Chem. Rev.* **1992**, *92*, 1355–1379. [CrossRef]
53. Sauerbrey, G. Verwendung von Schwingquarzen zur Wägung dünner Schichten und zur Mikrowägung. *Zeitschrift Für Physik* **1959**, *155*, 206–222. [CrossRef]
54. Sreeja, R.; Swaminathan, B.; Painuly, A.; Sebastian, T.V.; Packirisamy, S. Allylhydridopolycarbosilane (AHPCS) as matrix resin for C/SiC ceramic matrix composites. *Mater. Sci. Eng. B Solid-State Mater. Adv. Technol.* **2010**, *168*, 204–207. [CrossRef]
55. Kaur, S.; Riedel, R.; Ionescu, E. Pressureless fabrication of dense monolithic SiC ceramics from a polycarbosilane. *J. Eur. Ceram. Soc.* **2014**, *34*, 3571–3578. [CrossRef]
56. Wen, Q.; Xu, Y.; Xu, B.; Fasel, C.; Guillon, O.; Buntkowsky, G.; Yu, Z.; Riedel, R.; Ionescu, E. Single-source-precursor synthesis of dense SiC/HfC_xN_{1-x}-based ultrahigh-temperature ceramic nanocomposites. *Nanoscale* **2014**, *6*, 13678–13689. [CrossRef]
57. Proust, V.; Bechelany, M.C.; Ghisleni, R.; Beaufort, M.F.; Miele, P.; Bernard, S. Polymer-derived Si-C-Ti systems: From titanium nanoparticle-filled polycarbosilanes to dense monolithic multi-phase components with high hardness. *J. Eur. Ceram. Soc.* **2016**, *36*, 3671–3679. [CrossRef]
58. Schmidt, M.; Durif, C.; Acosta, E.D.; Salameh, C.; Plaisantin, H.; Miele, P.; Backov, R.; Machado, R.; Gervais, C.; Alauzun, J.G.; et al. Molecular-Level Processing of Si-(B)-C Materials with Tailored Nano/Microstructures. *Chem.-A Eur. J.* **2017**, *23*, 17103–17117. [CrossRef] [PubMed]

59. Ferrari, A.C.; Robertson, J. Interpretation of Raman spectra of disordered and amorphous carbon. *Phys. Rev. B* **2000**, *61*, 14095–14107. [CrossRef]
60. Pimenta, M.A.; Dresselhaus, G.; Dresselhaus, M.S.; Cançado, L.G.; Jorio, A.; Saito, R. Studying disorder in graphite-based systems by Raman spectroscopy. *Phys. Chem. Chem. Phys.* **2007**, *9*, 1276–1291. [CrossRef] [PubMed]
61. Sing, K.S.W.; Everett, D.H.; Haul, R.A.W.; Moscou, L.; Pierotti, R.A.; Rouquerol, J.; Siemienieska, T. Reporting physisorption data for gas/solid systems with special reference to the determination of surface area and porosity. *Pure Appl. Chem.* **1985**, *57*, 603–619. [CrossRef]
62. Lowell, S.; Shields, J.E.; Thomas, M.A.; Thommes, M. *Characterization of Porous Solids and Powders*; Springer: Dordrecht, The Netherlands, 2004.
63. Lee, H.R.; Kanezashi, M.; Shimomura, Y.; Yoshioka, T.; Tsuru, T. Evaluation and fabrication of pore-size-tuned silica membranes with tetraethoxydimethyl disiloxane for gas separation. *AIChE J.* **2011**, *57*, 2755–2765. [CrossRef]
64. Yoshioka, T.; Kanezashi, M.; Tsuru, T. Micropore size estimation on gas separation membranes: A study in experimental and molecular dynamics. *AIChE J.* **2013**, *59*, 2179–2194. [CrossRef]
65. Lee, D.; Zhang, L.; Oyama, S.T.; Niu, S.; Saraf, R.F. Synthesis, characterization, and gas permeation properties of a hydrogen permeable silica membrane supported on porous alumina. *J. Membr. Sci.* **2004**, *231*, 117–126. [CrossRef]
66. Gu, Y.; Oyama, S.T. High Molecular Permeance in a Poreless Ceramic Membrane. *Adv. Mater.* **2007**, *19*, 1636–1640. [CrossRef]
67. Ahn, S.J.; Yun, G.N.; Takagaki, A.; Kikuchi, R.; Oyama, S.T. Synthesis and characterization of hydrogen selective silica membranes prepared by chemical vapor deposition of vinyltriethoxysilane. *J. Membr. Sci.* **2018**, *550*, 1–8. [CrossRef]
68. Ren, X.; Tsuru, T. Organosilica-based membranes in gas and liquid-phase separation. *Membranes* **2019**, *9*, 107. [CrossRef]
69. Li, L.; Wang, C.; Wang, N.; Cao, Y.; Wang, T. The preparation and gas separation properties of zeolite/carbon hybrid membranes. *J. Mater. Sci.* **2015**, *50*, 2561–2570. [CrossRef]
70. Li, L.; Xu, R.; Song, C.; Zhang, B.; Liu, Q.; Wang, T. A review on the progress in nanoparticle/C hybrid CMS membranes for gas separation. *Membranes* **2018**, *8*, 134. [CrossRef] [PubMed]
71. Zeynali, R.; Ghasemzadeh, K.; Sarand, A.B.; Kheiri, F.; Basile, A. Performance evaluation of graphene oxide (GO) nanocomposite membrane for hydrogen separation: Effect of dip coating sol concentration. *Sep. Purif. Technol.* **2018**, *200*, 169–176. [CrossRef]
72. Nouri, M.; Ghasemzadeh, K.; Iulianelli, A. Theoretical evaluation of graphene membrane performance for hydrogen separation using molecular dynamic simulation. *Membranes* **2019**, *9*, 110. [CrossRef]
73. Li, Y.; Lin, L.; Tu, M.; Nian, P.; Howarth, A.J.; Farha, O.K.; Qiu, J.; Zhang, X. Growth of ZnO self-converted 2D nanosheet zeolitic imidazolate framework membranes by an ammonia-assisted strategy. *Nano Res.* **2018**, *11*, 1850–1860. [CrossRef]
74. Fang, M.; Montoro, C.; Semsarilar, M. Metal and covalent organic frameworks for membrane applications. *Membranes* **2020**, *10*, 107. [CrossRef] [PubMed]
75. Li, H.; Song, Z.; Zhang, X.; Huang, Y.; Li, S.; Mao, Y.; Ploehn, H.J.; Bao, Y.; Yu, M. Ultrathin, molecular-sieving graphene oxide membranes for selective hydrogen separation. *Science* **2013**, *342*, 95–98. [CrossRef] [PubMed]
76. Huang, L.; Lin, H. Engineering sub-nanometer channels in two-dimensional materials for membrane gas separation. *Membranes* **2018**, *8*, 100. [CrossRef]
77. Lasseuguette, E.; Malpass-Evans, R.; Carta, M.; McKeown, N.B.; Ferrari, M.C. Temperature and pressure dependence of gas permeation in a microporous Tröger's base polymer. *Membranes* **2018**, *8*, 132. [CrossRef]
78. Malpass-Evans, R.; Rose, I.; Fuoco, A.; Bernardo, P.; Clarizia, G.; McKeown, N.B.; Jansen, J.C.; Carta, M. Effect of bridgehead methyl substituents on the gas permeability of Tröger's-base derived polymers of intrinsic microporosity. *Membranes* **2020**, *10*, 62. [CrossRef]